International Journal of Technology 13(3) 518-532 (2022)
Received March 2021 / Revised June 2021 / Accepted January 2022

International Journal of Technology

http://ijtech.eng.ui.ac.id

Experimental and Computational Fluid Dynamics Investigations into the Effect of Loading Condition on Resistance of Hard-Chine Semi Planning Crew Boat

Soegeng Riyadi[1], Wasis Dwi Aryawan[1], I Ketut Aria Pria Utama[1*]

[1]*Department of Naval Architecture, Faculty of Marine Technology, Institut Teknologi Sepuluh Nopember, Kampus ITS Sukolilo, Surabaya 60111, Indonesia*

Abstract. Nowadays, the issue of energy efficiency in the maritime transportation sector has been strongly associated with the decreasing use of fossil energy and greenhouse gas emissions. Crew boats are one of the ship modes which consumes a lot of fuel in maritime transportation. This affects the number of exhaust gases released into the atmosphere. A study into the estimation of crew boat resistance was carried out experimentally using a towing tank, numerically using a CFD methodology, and then compared with Savitsky's method. Measurements were taken in calm waters under even keel and trim scenarios, considering load variation had been adjusted for. Determining the correct load position affected the LCG (Longitudinal Center of Gravity) and VCG (Vertical Center of Gravity) parameters, affected trim, and decreased crew boat resistance. Overall results showed that the experimental test, CFD method, and the empirical estimation from Savitsky were in good agreement with average errors up to 3%. The calculation results demonstrated that trim had a greater influence on decreasing resistance up to 3.062% than even keel position. Furthermore, the shifting of LCG had a more significant effect than that of VCG in the context of resistance changes.

Keywords: Computational Fluid Dynamics (CFD); Crew boat; Energy efficiency; Loading condition; Resistance; Semi-planning

1. Introduction

Crew boats are very important to the shipping industry as they provide the connection between a base onshore and offshore installations, such as drilling rigs, or designated anchorages that serve hundreds of ships at a time (Karanassos, 2016). Companies that operate fleets of offshore structure platforms need boats to transport employees and operators to and from the platforms regularly. These crew boats are also employed for modest constructions or minor changes on the platform thus they are utilized to transport teams of workers and their equipment (El-Reedy, 2021).

Currently, energy efficiency in the transportation sector is an absolute necessity. The contribution of energy demands in the transportation sector is about 21% of the total energy needed in the world, whereas sea transportation energy contributes approx. 6% of the total transportation energy demand (British Petroleum, 2020). The impact of the energy used in maritime transportation is directly proportional to the production of exhaust gases

*Corresponding author's email: kutama@na.its.ac.id, Tel.: +62-31-5964182, Fax.: +62-31-5964182
doi: 10.14716/ijtech.v13i3.4597

and pollution, which are both current problems in the environment. Crew boats compete directly with helicopters, therefore they are built with a high-speed planning hull and lightweight aluminium to overcome resistance (Latorre, 2003) and some crew boats are intended to carry passengers and cargo while operating in a semi-planning mode. Crew boat as the object of this research is a type of marine transportation that focuses its operations on speed and energy efficiency. Energy efficiency in marine transportation is very dependent on operational optimization among the hull of the ship, engine, propulsion system, and the routes.

Trim optimization was one of the effective measures to reduce fuel consumption (Molland et al., 2014). Reichel et al. (2014) studied the physics behind the changing of propulsive power when trimming a vessel to detect the origin of the changes. Islam and Soares (2019) presented trim optimization at different speeds and drafts could be a convenient and effective way for vessels to improve efficiency. Le et al. (2021) described the physical phenomena of a ship's resistance shifting as the trim state changed. The residuary resistance coefficient acting on the hull resistance was found to be the major effect resulting in changing propulsive power when a vessel was trimmed. Residual resistance is made up of wave resistance, which refers to the energy loss produced by the vessel's waves, and viscous pressure resistance (Molland et al., 2017).

One of the powerful tools to investigate the problems above was by using the computational fluid dynamics (CFD) method (Bertram, 2011). Sherbaz and Duan (2014) demonstrated that trim had a pronounced increasing effect on resistance during bow trim at MOERI container ships (KCS). The effect on resistance is varying during stern trim and the optimum trim point is 0.02 m trim by stern. The study of viscous and wave-making components reveals that viscous resistance changes slightly with a change in trim whereas trim had a dominant effect on the wave-making resistance. Kazemi and Salari (2017) provided a computational and experimental hydrodynamic study for a hard-chine planning boat under a variety of loading variables and speeds. The comparison of numerical and laboratory findings revealed a high degree of agreement between them. Furthermore, CFD applications are used in the evaluation of water flows regarding the effects on ships (Suastika et al., 2017; Utama et al., 2021a), they presented that the CFD calculations and model testing correlate quite well for overall ship resistance in calm water.

CFD simulation was utilized in this research to determine resistance, and tank tests were performed to validate the results. The main objective was to analyze the drag on the crew boat due to the center of mass movement. The stages were as follows; firstly, comparing the geometric properties of the crew boat model using CFD and experimental data. Secondly, the CFD solver was briefly introduced, followed by the numerical setup consisting of mesh generation and boundary conditions. Thirdly, the CFD verification technique was applied in the validation of the numerical approach, and it was accomplished by comparing the resistance values obtained from CFD, Savitsky, and experimental methods. Finally, by following verification and validation, CFD analysis was performed on 3 (three) longitudinal loads and 3 (three) vertical loads at the cargo deck and there were differences in trim on the crew boat. Calculation of the trim effect to identify the optimal load configuration in terms of reducing ship resistance was carried out and discussed.

2. Methods

This research focused on crew boats with varying loads that affected the placement of the center of mass. Then, using the CFD method, an analysis of the resistance at Fr=0.117 to 0.701 (semi planning) was performed, with verification using the Savitsky technique and validation using an experimental model at Hydrodynamics Laboratory at the Institut

Teknologi Sepuluh Nopember. Furthermore, it was developed with six adjustments in the center of mass, three vertically and three horizontally, utilizing the CFD approach.

2.1. Ship Geometry

Principal particulars of the crew boat and model are presented in Table 1 and its geometry is shown in Figure 1 consisting of (i) buttock plan, (ii) body plan, and (iii) breadth plan. Furthermore, the body plan showed the shape of the section with hard chine form as a typical type of semi-planing hull. This model was analyzed at 6 speeds of variation, i.e., at *v* (m/s) = 0.982, 1.964, 2.947, 3.929, 4.911, 5.893 which correlated to Fr = 0.117, 0.234, 0.350, 0.467, 0.584, 0.701.

Table 1 Principal particular of crew boat model

Dimension		Model	Unit
Length Over All	(LOA)	0.716	m
Length of Waterline	(LWL)	0.672	m
Breadth	(B)	0.170	m
Draft	(T)	0.036	m
Wetted surface Area	(WSA)	0.107	m^2
Displacement		1.949	kg
Block Coefficient	(C_B)	0.519	

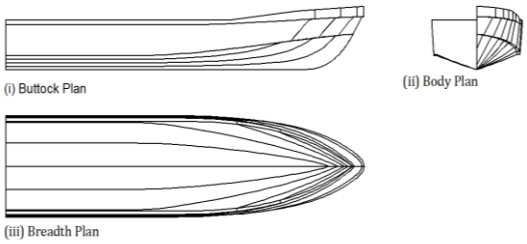

Figure 1 The crew boat body lines

2.2. Computational Fluid Dynamics

2.2.1. Numerical Model

CFD simulations were carried out to calculate the ship resistance for a variety of ship parameters such as speed, trim condition, and center of gravity location. A finite volume technique was utilized in CFD simulations using Numeca Fine/Marine® (FVM). For simulating turbulent multiphase flows with proper boundary conditions, the ISIS-CFD code of the package solved the RANS equations with acceptable boundary conditions. Modeling of wave generation was done using the volume of fluid (VOF) technique to determine the free surface boundary. The numerical problem was controlled by Continuity and RANS Equations. The ship's fluid flow is incompressible. The numerical issue was controlled by continuity and RANS equations (1) and (2):

$$\frac{\partial U_i}{\partial x_i} = 0 \tag{1}$$

$$\frac{\partial U_i}{\partial t} + U_j \frac{\partial U_i}{\partial x_j} = \frac{\partial \hat{p}}{\partial x_i} + \frac{\partial}{\partial x_j}\left[\mathrm{Re}_{eff}^{-1}\left(\frac{\partial u_i}{\partial x_j} + \frac{\partial u_j}{\partial x_i} \right) \right] + S_i \tag{2}$$

where $U_i = (u, v, w)$ denoted the Reynolds-averaged velocity components; $x_i = (x, y, z)$ represented the independent coordinate directions; the term *Si* represented the mean strain-rate tensor for a body force, the piezometric pressure $\hat{p}$ and the $\mathrm{Re}_{\mathrm{eff}}$ were effective Reynolds numbers.

The SST model combined the k-ω benefits models to provide an optimum model formulation for many applications. The merging function F1 was introduced, which was one near the solid surface and zero away from the wall. It activated the k-ω wall region and the k- ε flow model. The k- ω appealing model's near-wall performance may be utilized without the possible mistakes caused by its free stream sensitivity, it gave highly accurate predictions of the onset and the amount of flow separation under adverse pressure

gradients (Menter, 1994). These were the modeled equations for turbulent kinetic energy, k and turbulence frequency ω were as follows:

$$\frac{\partial(\rho k)}{\partial t}+\frac{\partial(\partial u_j k)}{\partial x_j}=P-\beta^*\rho\omega k+\frac{\partial}{\partial x_j}\left[(\mu+\sigma_k\mu_t)\frac{\partial k}{\partial x_j}\right] \quad (3)$$

$$\frac{\partial(\rho\omega)}{\partial t}+\frac{\partial(\rho u_j\omega)}{\partial x_j}=\frac{\gamma}{v_t}P-\beta\rho\omega^2+\frac{\partial}{\partial x_j}\left[(\mu+\sigma_\omega\mu_t)\frac{\partial\omega}{\partial x_j}\right]+2(1-F_1)2\rho\sigma_{\omega2}\frac{1}{\omega}\frac{\partial k}{\partial x_j}\frac{\partial\omega}{\partial x_j} \quad (4)$$

The SST model was ranked as the best accurate model in its class by Bardina et al., (1997), according to a NASA Technical Memorandum published in 1997. This thing could also be found in the extensive study on trimaran ships that was performed by Utama et al., (2021a).

2.2.2. Computational Domain and Boundary Condition

Numeca Fine/Marine® states the boundary conditions are presented in Figure 2. Reducing computing complexity and demand could be accomplished by representing only half of the hull (the starboard side) (ITTC, 2014a). One of the domain faces of the model was aligned along the centerline of the domain, to mimic the other half of the model. For the drawing, it should be mentioned that on certain figures, the mirror reflection of the ship and domain were shown on the port side.

The computational domain is illustrated in Figure 3. However, to the ship's symmetry, exactly half of the ship was represented. This was located 1.0 L upstream from the vessel, and it was located 3.0 L downstream from the vessel. The entrance and outlet were in the same location. The sidewall measured 1.50 L on either side of the vessel. The bottom wall was 1.50 L below the vessel, while the top wall was 0.50 L above the vessel (L was the length between the perpendiculars, LBP).

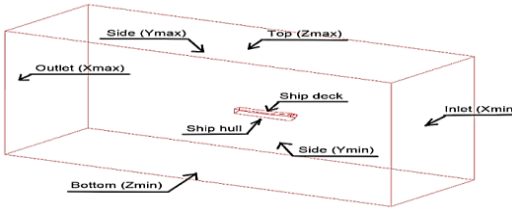

Figure 2 A sketch of the boundary condition

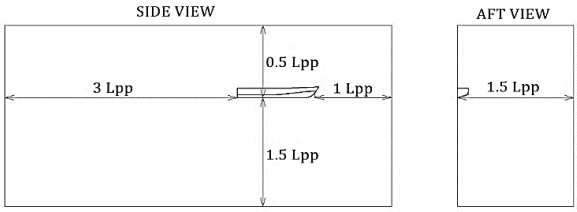

Figure 3 Computational domain for crew boat simulation

2.2.3. Mesh Generation

For a high number of cells, the total resistance was anticipated to approach an asymptotical value. The number of cells of 3.5×10^6 was chosen as the most optimal number of cells in this research because of the restricted capacity of available hardware. The number of cells was determined using a grid independence study (Anderson, 1995), as shown in Table 2. The meshing arrangement is presented in Figure 4.

Table 2 Simulation of a cell by grid independence

Run number *N*	Number of cells *N*	Total Resistance Coefficient	Percent error [%]
1	462,271	0.2939	-
2	931,892	0.3406	13.71%
3	1,804,625	0.3685	7.56%
4	3,496,660	0.3721	0.97%

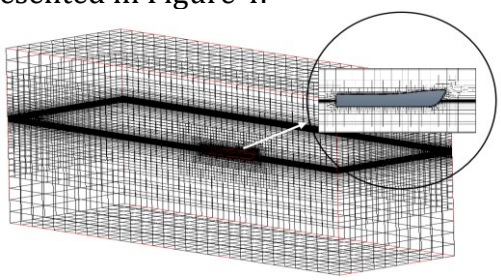

Figure 4 Mesh for CFD simulation

The grid convergence research was determined by the ITTC's guideline for uncertainty analysis (ITTC, 2017). The convergence study was carried out using three different mesh resolutions that were divided into three categories: coarse, medium, and fine mesh as shown in Table 3. The Solutions were used to define the convergence ratio as equation (5) follows:

$$Ri = \varepsilon_{21}/\varepsilon_{32} \quad (5)$$

Where:

Ri = Convergence Ratio; ε_{21} = Difference of estimation between medium-fine; ε_{32} = Difference of estimation between coarse-medium

Before evaluating the projected value derived from the equations above, it was necessary to understand the convergence conditions of this system. The following were the convergence criteria that must be met:

1. Monotonic convergence: $0 < Ri < 1$
2. Oscillatory convergence: $Ri < 0$
3. Divergence: $Ri > 1$

To estimate the errors and uncertainties in the case of monotonic convergence, the extended Richardson Extrapolation method was used for the estimation of the mesh error. In the case of oscillatory convergence, the findings demonstrated that there were some oscillations. Finally, in the case of divergence, the findings diverged while mistakes and uncertainties were difficult to identify or quantify.

Table 3 Three varying mesh resolution details

Detail	Fine (1)	Medium (2)	Coarse (3)
Number of Elements (NE)	3,496,660	1,804,625	931,892
Drag coefficient ($x10^{-3}$) (C_T)	0.3721	0.3685	0.3406

The suggested value for the refinement ratio, r_i, was $\sqrt{2}$, since the number was high enough to be a critical parameter. Table 4 displayed the results of calculations based on the formula from the utilized equation section, ensuring that the grid independence study had a monotonic convergence with ri =0.1290 and that it was in compliance with the ITTC's requirements (ITTC, 2017).

Table 4 The uncertainty analysis performed for crew boat

Outcome	Equation	Value
Refinement ratio	$r_{12}=NE_1/NE_2$	1.9376
	$r_{23}= NE_2/NE_3$	1.9365
Difference of estimation	$\varepsilon_{21}=C_{T2} - C_{T1}$	-0.0036
	$\varepsilon_{32} = C_{T3} - C_{T2}$	-0.0279
Convergence	$r_i=\varepsilon_{21}/\varepsilon_{32}$	0.1290
Order of accuracy	$p=\ln(\varepsilon_{21}/\varepsilon_{32})/\ln(r_i)$	3.0957
Extrapolated relative error	$e_{21}= \varepsilon_{21}/r_i^p-1$	-0.0013
	$e_{32}= \varepsilon_{32}/r_i^p-1$	-0.0101
Grid convergence index (GCI)	$GCI_{21}=Fs\lvert e_{21}\rvert$	0.0016
	$GCI_{32}= Fs\lvert e_{32}\rvert$	0.0132

A layer with a high aspect ratio was inserted into the anisotropic cells subdivision to get a high enough resolution of the flow. For cells close to the wall, it was necessary to take into account the variations in the wall y^+, according to equation (6):

$$y^+ = \frac{\rho u_\tau y_{wall}}{\mu} \quad (6)$$

In the simulation, the value of y^+ is given by C-Wizard and the length between the perpendiculars (LBP) uses the Lref reference line. The number of y^+mentioned in ITTC (2014c), thus by the C-Wizard recommendation 30 < y^+<80 in which the strong agreement between model testing and CFD calculations for total ship resistance in calm water results in a high degree of trust (Marintek, 2021).

2.3. Savitsky Method

The planing hull has a changeable deadrise angle throughout its length. The variable deadrise may be included in the equations (7-9) by using effective deadrise and beam at the LCG section (Savitsky, 2003), as illustrated in Figure 5. Resistance calculation of crew boat was carried out using the Maxsurf resistance in conjunction with the Savitsky technique (Bentley Systems. Inc., 2018).

$$D = D_p + \frac{D_f}{\cos\tau} \tag{7}$$

$$D_p = \Delta \tan\tau \tag{8}$$

$$D_f = \frac{C_f v^2 (\lambda b^2)}{2cos\beta^4} \tag{9}$$

Where:

D = Total drag (N); D_p = Pressure drag (N); D_f = Friction drag (N); τ = trim angle (deg); Δ = load (kg); C_f = Friction Coefficient; λb^2 = Viscous Drag (N); v = velocity (m/s); β = deadrise angle (deg).

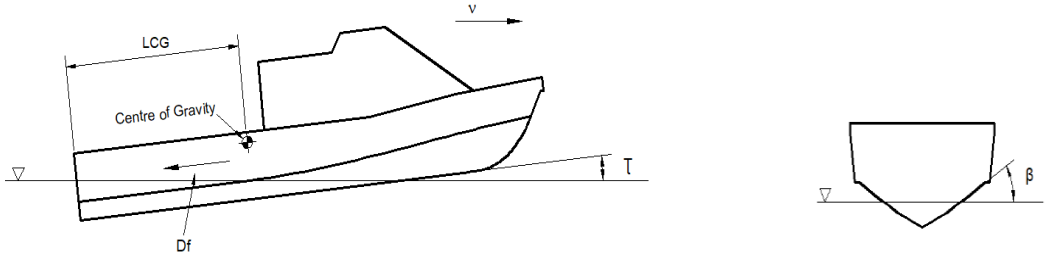

(a) Side view (b) Front view

Figure 5 Ship Planning Hull

2.4. Resistance Calculation at Trim Condition

The motion equation used two coordinate systems. One was the body-fixed coordinate system (Gξζ) at the center of gravity (CG). The ζ -axis was parallel to the baseline and positive. The -axis was parallel to the baseline and positive downward. The second system (OXZ) was a stationary straight coordinate system that moved with the boat's forward speed. The origin of this coordinate system was where the CG normal line intersects the calm water surface. Derived from the X-axis, the Z-axis was parallel to and positive ahead of the calm water surface. Figure 6 depicts the boat's forces and moments in motion. The hydrodynamic force (F_{HD}), buoyancy force (F_B), and associated moments are all included (M_{HD} and M_B). Considering that the forces of drag and push do not affect movement, the solution for motion under steady-state conditions may be written as equations (10) and (11):

$$\Sigma F_z = 0 \quad \rightarrow \quad W - F_{HD} - F_B = 0 \tag{10}$$

$$\Sigma M_G = 0 \quad \rightarrow \quad M_{HD} + M_B = 0 \tag{11}$$

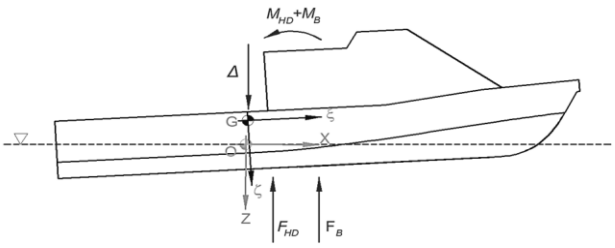

Figure 6 Coordinate system and force acting in Planing Hull

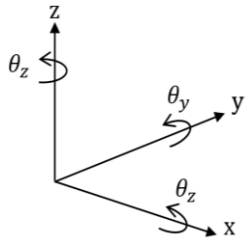

Figure 7 Coordinate system six degrees of freedom of body

The first equation represented the equilibrium in the Z direction, whereas the second equation described the equilibrium of the pitch moments about CG. Ghadimi et al., (2017) explained the importance to determine these forces to establish the equilibrium state.

The calculation of ship resistance involved the interaction between hull and fluid, which was commonly known as FSI (Fluid-Structure Interaction)(Diez et al., 2020). These were obtained by calculating the vessel's equations of motion and rotation under the influence of the surrounding fluids and gravity. The number of directions a body may move and rotate is termed its degrees of freedom (DOF).

The coordinate system illustrates a rigid body's six degrees of freedom, as shown in Figure 7. These include translation and rotation along three axes in the x, y, and z parameters. In this study, crew boat resistance analysis was carried out in trim conditions which were influenced by heave and pitch only. Newton's second law described the translational motion of the center of gravity for a rigid body, as equation (12):

$$F = m\frac{dv}{dt} \tag{12}$$

Where m was the mass, *v* was velocity and F was the sum of forces acting on the body. Then, the rotation of the body, expressed in body coordinates, was described by Euler's equations (13):

$$\tau = M\frac{d\omega}{dt} + \omega\, x\, (M.\omega) \tag{13}$$

Where ω was the angular velocity of the body and τ was the resultant torque acting on the body. Furthermore, M was a tensor of the moments of inertia and it was expanded into equation (14):

$$M = \begin{bmatrix} M_{xx} & M_{xy} & M_{xz} \\ M_{yx} & M_{yy} & M_{yz} \\ M_{zx} & M_{zy} & M_{zz} \end{bmatrix} \tag{14}$$

2.5. Tank Test

2.5.1. Model Resistance Test

Towing-tank experiments were performed with the dimension of the tank was as follows: length = 50.0 m, width = 3.0 m, maximum water depth = 2.0 m and maximum towing speed = 4.0 m/s.

A model of the ship was made of fiberglass reinforced plastic (FRP) that had been painted and coated with resin. The geometrical scale between the model and the prototype was 1:26.57, and the scale was appropriate in terms of the towing tank's speed and capability. Bertram (2011) explained the scaling procedure's computation in detail. In addition, this procedure is already used in study on multihull ship resistance (Luhulima et al., 2021). In the tests, the Froude scaling was used to differentiate between the full size and the model ship. A load cell was used to test the resistance of the ship. Before conducting the test, the load cell was calibrated by applying a mass of 0.5 kg to the load cell. The model was

tested in the towing tank at sufficient speed from Fr = 0.117 to 0.701. Figure 8 illustrates a ship model attached to a carriage and prepared for towing in the towing tank.

Figure 8 Ship model towed in a towing tank

2.5.2. Uncertainty Test Resistance Model

The model was measured in a controlled environment. Using two clamping mechanisms, the ship model's trim and sinkage were controlled. The integration of uncertainty evaluations in all stages of the experimental process was given special attention, as recommended by ITTC (2014a, 2014b), as follows: wetted area, speed, water temperature, dynamometer, and repeated tests. The analysis of all major uncertainty components associated with the total resistance is combined to get the overall standard uncertainty using the RSS approach using equation (15):

$$u_c' = \sqrt{(u_1')^2 + (u_2')^2 + (u_3')^2 + (u_4')^2 + (u_5')^2} \quad (15)$$

Where:

$(u_1')^2$ was the relative standard uncertainty components of resistance related to the hull geometry
$(u_2')^2$ was the uncertainty of resistance resulting from the towing speed
$(u_3')^2$ was the relative standard uncertainty of resistance
$(u_4')^2$ was the uncertainty component of the resistance resulting from the calibration of the dynamometer is estimated by standard error estimation (SEE)
$(u_1')^2$ was the standard uncertainty component from single test tests

Then, the standard uncertainty of the resistance was increased for the classification accuracy (t) was used equation (16):

$$U_{p(R_T)=k_p u_c'(R_T)} \quad (16)$$

where kp was the coverage factor

The combined standard uncertainty is calculated using RSS (Root-Sum-Square) as shown in the accompanying Table 5.

Table 5 The combined uncertainty (Fr = 0.701)

R_T	Type	Uncertainty (%)	Remark
Wetted Area	B	0.12	Minor
Speed	B	0.035	Negligible
Water Temperature	B	0.012	Negligible
Dynamometer	A	0.085	Negligible
Repeat test, Deviation	A (N=3)	1.57	Dominant
Combined for a single test		1.65	
Repeat test, Deviation	A (N=3)	0.45	Minor
Combined for repeat mean		0.21	

The expanded standard of uncertainty level is determined by using the following formula within a confidence level of 95% as shown in Table 6.

Table 6 Resistance Coefficient with expanded uncertainty (kp=2) measured in freshwater

Fr	U' (t=2)	C_T at T = 27^{0}C
0.701	0.13%	0.3685±0.13%

The crew boat model's uncertainty was examined at operating speed (Fr=0.701). The measuring system should be updated beginning with the dominant uncertainties and progressing to minor uncertainties. The statistical analysis that followed quantifies values with mean differences from the single to the repeated mean experimental test instance, which had a standard deviation of 0.13%. The case study model was examined at Fr = 0.701 and found to be an acceptable result (Utama et al., 2021b).

2.6. Verification and validation

2.6.1. Resistance

Numerical calculation with CFD was verified and compared with those obtained methods using Savitsky's model and experimental data (towing-tank experiments). It can be seen in Figure 9 (a) that spray is generated on the front part at the speed with Fr = 0.701 and CFD visualization shows the same pattern, in Figure 9 (b). Further, the spray is thrown away out of the ship model and this occurs because of the existence of the front chine.

The effect of the chine was to produce lift in the front area, which increased as the speed raised. Kelvin wave pattern was produced behind the vessel together with the formation of eddies. The result of total resistance is plotted in Figure 10 and shows the use of three methods: CFD, tank test, and Savitsky. The validation findings revealed a relatively minor difference, with an average difference of 0.2% between CFD and Experiment and 3.4% between CFD and the Savitsky method.

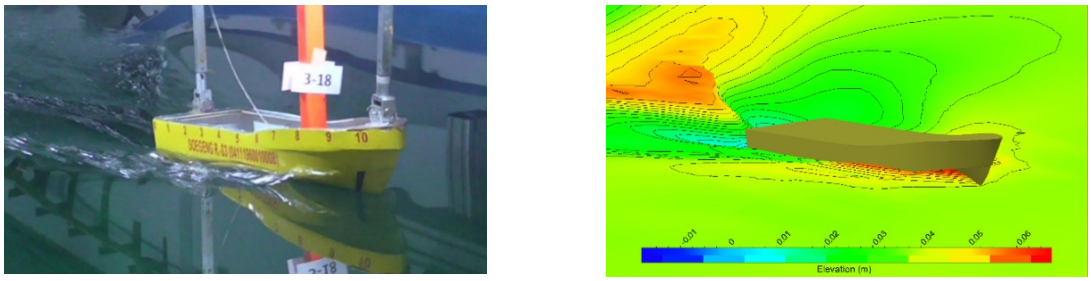

(a) Towing Tank Experiment (b) CFD Result

Figure 9 Visualization comparison in Fr = 0.701

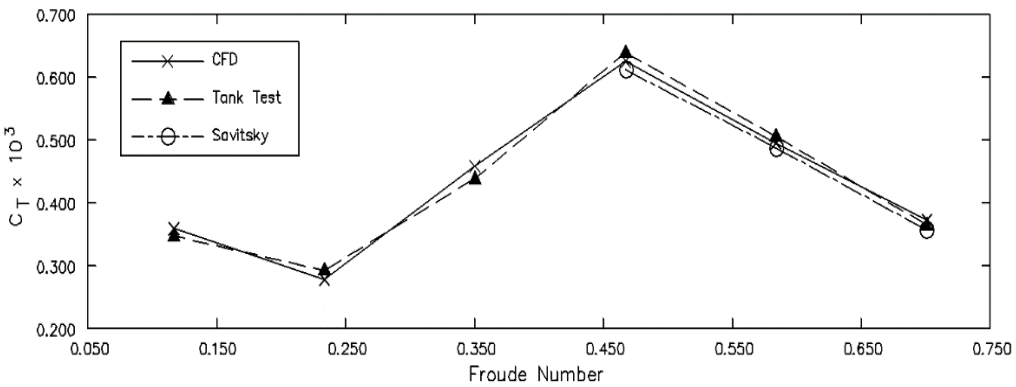

Figure 10 Total resistance comparison among tank test, CFD, and Savitsky method

2.7. Loading Condition Simulation

Energy efficiency by indicator resistance with focusing on shifting load from initial load position in the deck cargo area. The adjustment in loading condition affects the initial trim described in Table 8 and the position of the load center of gravity can be found in Figure 11. The running models in CFD with a variation of every load case and speed correlate in Froude Numbers.

Table 8 Variation of load case shifting position (measured from aft perpendicular and baseline)

LC	Load Position			Displacement	Load	Draft			CG		
Load Case		LCG [m]	VCG [m]	[Ton]	[Ton]	Aft [m]	Midship [m]	Fore [m]	LCG [m]	TCG [m]	KG [m]
LC 1	Load Design	3.20	2.50	36.40	3.70	0.999	0.941	0.882	6.53	0.00	1.92
LC 2	Load Shifting		+ 0.90	36.40	3.70	0.999	0.941	0.882	6.53	0.00	2.01
LC 3	Load Shifting	- 1.60		36.40	3.70	1.036	0.93	0.831	6.37	0.00	1.92
LC 4	Load Shifting	- 1.60	+ 0.90	36.40	3.70	1.036	0.934	0.831	6.37	0.00	2.01
LC 5	Load Shifting	+ 1.60		36.40	3.70	0.976	0.945	0.914	6.63	0.00	1.92
LC 6	Load Shifting	+ 1.60	+ 0.90	36.40	3.70	0.976	0.945	0.914	6.63	0.00	2.01

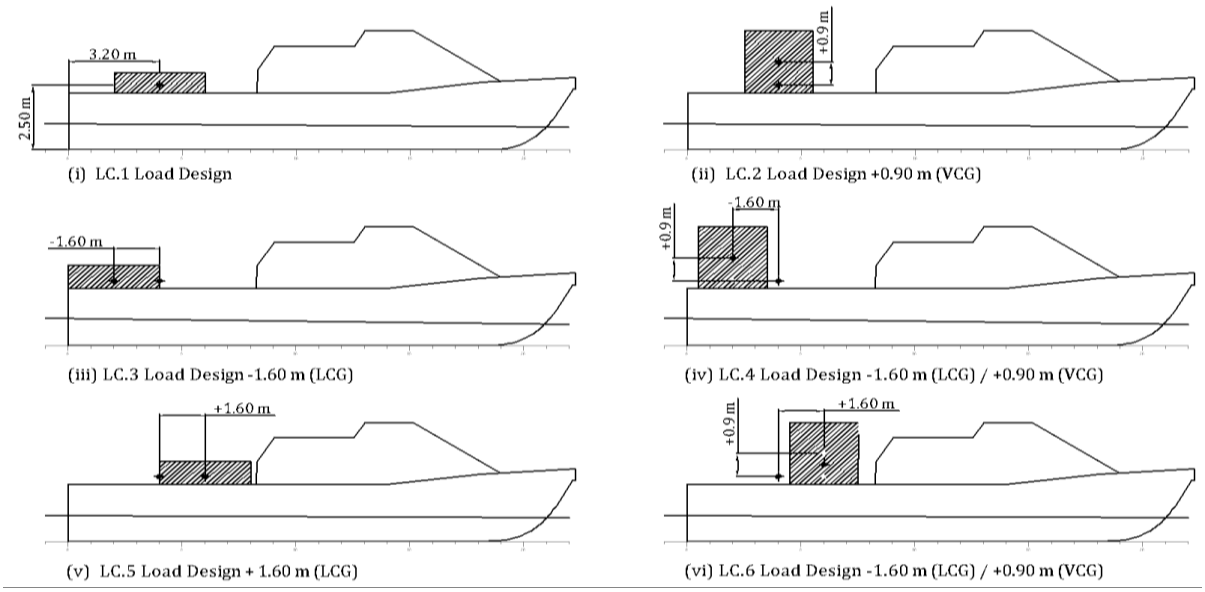

Figure 11 Side view of shifting the position of load

3. Results and Discussion

The impact of positioning the cargo on the stern of the ship, which was the output of Maxsurf, resulted in distinct starting conditions for each load instance. In this investigation, the reference loading condition was LC1. The simulation findings show that the difference in the ship's first trim under the beginning circumstances for each LC, namely LC1, LC2, and LC3 are 0.40, 0.69, and 0.21°, respectively. The higher the angle, the more the weight is placed behind the resultant angle, and the reverse effect applies when the load is carried forward.

A coefficient of total resistance curve was produced from the CFD simulation for each load case and Froude number as shown in Figure 12. The VCG differences vary greatly, while the variation among LCG differences is just slightly different. Therefore, of course, there are two identical LCG references. The differences in C_T (across all the pairs) are about

equal to -0.0253 for LC5 and 0.0397 for LC3 at the first Fr. The higher the Fr, the smaller the difference appears between LC3 and Fr 0.700. At LC3, it is zero, whereas, at Fr 0.700, it is -0.0035. In other words, the lower the Fr, the less influence the charge has on the contributor.

A percentage deviation calculation was conducted using the reference to LC1 as illustrated in Figure 13 to find out the specifics of the discrepancies in each LCG pair. The loading applied behind LC1 increased C_T by 7.102% at Fr = 0.117 and progressively declined to 5.098% at Fr = 0.700 in the LC3 pair. The loading of the charge in front of LC1 in the LC5 pair, on the other hand, generated a C_T reduction impact of 4.031% at Fr=0.117, which was reduced with rising Fr. As a result, at Fr = 0.700, it drops to LC1, resulting in a 3.062% reduction in C_T.

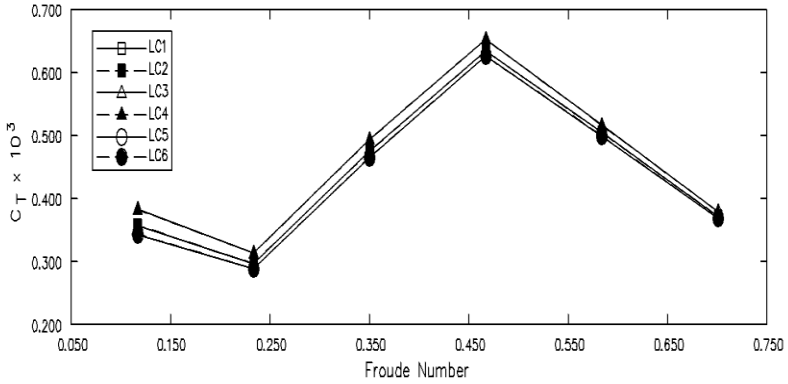

Figure 12 Coefficient of Total resistance (C_T) calculation with 6 LCs

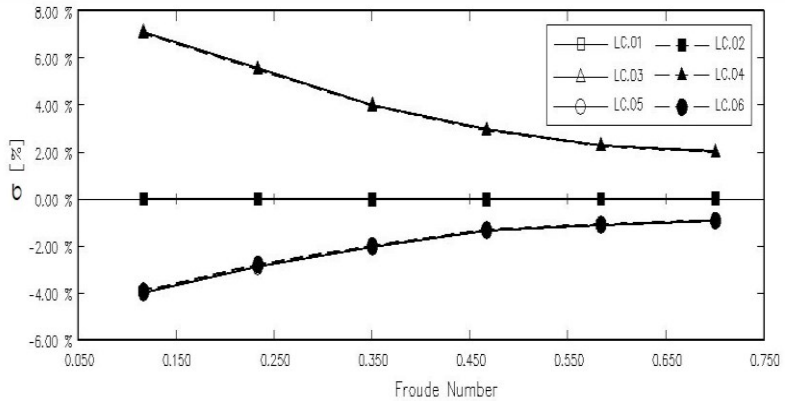

Figure 13 Total resistance coefficient relative to percent difference with reference LC.1

The impact of load transfer on wave elevation is seen in Figure 14. The side area of the ship with reference LC1 obtained in the LC3-LC4 pair had a wide wave area, but the LC5-LC6 pair had a lower wave area, although this was not statistically significant. The transom demonstrated that the wave pattern was shorter than the reference LC1 for LC3-LC4 and vice versa for LC5-LC6. Spray waves that entered the bow in the LC3-LC4 pair appeared to be larger than those that entered the bow in the other pairings. LC3-LC4 had a larger stern wave than the other pairs, therefore when evaluated from the perspective of the wave elevation phenomena, LC3-4 had a larger C_T and opposite LC5-LC6 had a smaller C_T than the reference LC1-LC2. These are the phenomena that occur during the semi-planing stage. Likewise, the stern wave system exhibits the same characteristics, with the high wave causing the ship's stern to sink even further.

Furthermore, it can be observed in Figure 15, which shows the contribution to hydrostatic pressure on the ship's bottom, that the impact of moving cargo followed a similar pattern. There were many items in the front region of the ship with a pressure range

of 200 N/m2, with the LC3-LC4 pair having a bigger area than LC1-LC2, and the LC5-LC6 pair having the reverse. The trim effect created negative pressure in the ship's rear region, resulting in a component of drag pressure. The contribution to the difference in LCG and VCG changes is not stated clearly.

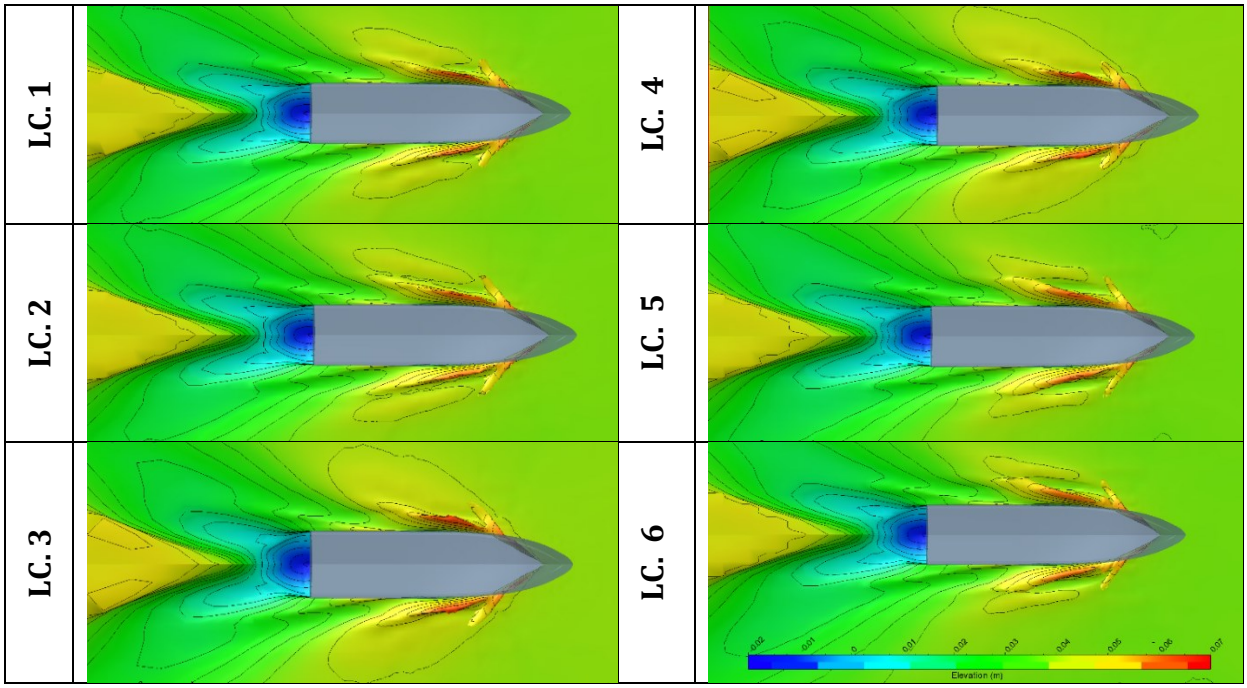

Figure 14 Wave elevation impact of load case in speed 1.796 m/s (Fr=0.701)

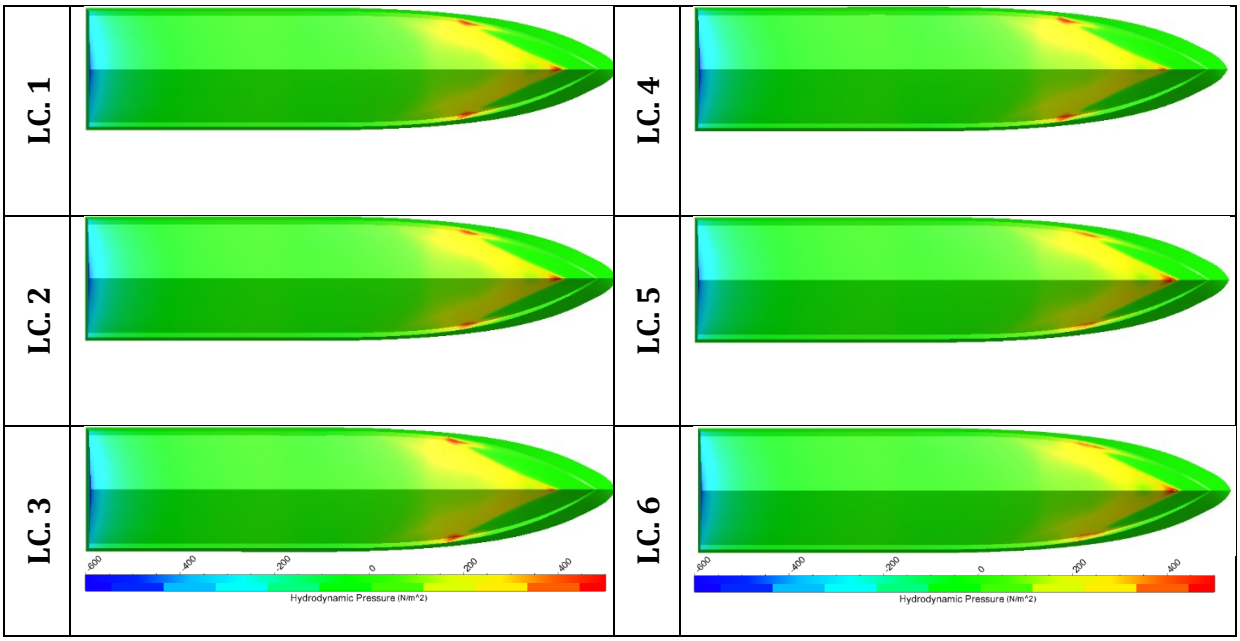

Figure 15 Hydrodynamic Pressure at the bottom surface at a speed of 1.796 m/s (Fr=0.701)

Lloyd Register of Shipping developed a manual of representative trim, which was made using the CFD method, and applied in SEATRIM®SOFTWARE as described by Reichel et al (2014). The operational recommendation was grouped into 4 (four) conditions, which was converted from the resistance discrepancy, namely optimal (<0,1%), good (0,1% <σ <0,2%), fair (0,2% <σ <0,4%), dan avoid (> 0,4%), and can be seen in Table 9.

Table 9 Range of trim recommendation converted from the resistance differences through LC simulation

Draft (aft-fore) [m]		0.976-0.914	0.976-0.914	0.999-0.882	0.999-0.882	1.036-0.831	1.036-0.831
KG [m]		1.92	2.01	1.92	2.01	1.92	2.01
Froude Number	0.117-0.223	Optimal 0.0%	Good 0.1%	Fair 3.3%	Fair 3.2%	Avoid 9.4%	Avoid 9.3%
Froude Number	0.350-0.467	Optimal 0.0%	Good 0.1%	Good 1.6%	Good 1.6%	Avoid 4.9%	Avoid 4.9%
Froude Number	0.584-0.701	Optimal 0.0%	Optimal 0.0%	Good 1.1%	Good 1.0%	Fair 3.2%	Fair 3.2%

In the group with Froude Number, the mean C_T of each group with draft conditions and KG were compared with other conditions. Thus, C_T with the lowest value became the reference as the optimal condition. They were grouped into criteria according to the Lloyd Register of Shipping using IMO (2016) reference. It allowed the crew to examine the ship's condition (aft and fore drafts) as well as the KG condition of the current ships. The ship's crew could set an operating speed pattern or undertake cargo shifts to optimize trim. Trim optimization was regarded as one of the simplest and easiest techniques for improving ship performance, specifically ship resistance (Lyu et al., 2018) and reducing fuel consumption (Sherbaz & Duan, 2014). Trim optimization at various speeds and drafts may be a simple and efficient method for boats to reduce resistance for increasing efficiency energy, decreasing fuel consumption, and restricting hazardous emissions (Islam & Soares, 2019). The decrease in greenhouse gas emissions was one of the environmental advantages of the fuel savings (Abouelfadl & Abdelraouf, 2016).

4. Conclusions

The current study has provided a computational and experimental hydrodynamic analysis of a crew boat under a variety of loading situations and speeds to validate and verify the results. The great degree of agreement between model testing and CFD predictions for total ship resistance in calm water has resulted in a high degree of confidence in the CFD results. The impact of longitudinal and vertical load variations was investigated on a model scale, with the findings of the tank test serving as confirmation of the results of the CFD output model construction. With the speed at Fr. 0.117, 0.467, and 0.701, the discrepancies differed, respectively 3.22%, 4.48%, and -2.04%. The initial conditions for the LC1-LC2, LC3-LC4, and LC5-LC6 pairings were 0.40 deg., 0.69 deg., and 0.21 deg., respectively, due to the influence of weight on the crew boat. There were three sets of C_T lines since each pair of LC groups produced comparable C_T. The differences to LC1 used as a reference are 0.0136 and -0.0172 at Fr=0.117, and 0.0039 and -0.0049 at Fr=0.701. The impact of changing placement has been less as Fr increases. At Fr=0117, the effect of VCG has changed in each LC with the same LCG having the least effect, 0.059% to 0.085%. The optimal condition for investigating operational speed, Fr=0.700, was obtained in the LC5-LC6 pair since C_T is lowered between 0.908% and 3.062% of the reference LC. This may also be observed in the LC pair's wave elevation for the smaller spray wave and stern wave. A similar effect may be achieved by using hydrostatic pressure spray. Consequently, it was discovered that shifting the position of the crew boat to the front resulted in less resistance than shifting the position to the back of the ship. The implementation of the investigation findings has been enabling the ship's crew to make better decisions about how to set the ship's speed and load position. Thus, by implementing

this, it can serve as an operational guide for reducing total ship resistance and hence exhaust gas emissions.

Acknowledgement

The authors wished to thank the Ministry of Research, Technology, and BRIN for the Doctoral Program Research Grant of the year 2020 under contract number 1238/PKS/ITS/2020. The authors also thanked Mr. Langgeng Condro, Mr. Achmad Sutiyo, and Mr. Rudie Aminudin for their help in experimental model tests.

References

Abouelfadl, A.H., Abdelraouf, E.E.Y., 2016. The Impact of Optimizing Trim on Reducing Fuel Consumption. *Journal of Shipping and Ocean Engineering*, Volume 6, pp. 179–184

Anderson, J.D., 1995. *Computational Fluid Dynamics: The Basics with Applications.* Mechanical Engineering Editions. New York, USA: McGraw-Hill, pp. 526–532

Bardina, J.E., Huang, P.G., Coakley, T.J., 1997. Turbulence Modeling Validation. *In*: 28th Fluid Dynamics Conference. https://doi.org/10.2514/6.1997C2121

Bentley Systems Inc., 2018. *User Manual: MAXSURF Resistance.* MAXURF Connect Edition V22. USA: Bentley Systems Inc.

Bertram, V., 2011. *Practical Ship Hydrodynamics*. 2nd Edition. USA: Elsevier Science

British Petroleum, 2020. Carbon Emissions from Energy Use are The Largest Source of Greenhouse Gas Emissions, Energy Outlook 2020 Edition. Available at: https://www.bp.com/content/dam/bp/businesssites/en/global/corporate/pdfs/energy-economics/energy-outlook/bp-energy-outlook-2020.pdf.

Diez, M., Lee, E.J., Powers, A.M., Fullerton, A.M., Lewis, R.R, Harrison, E.L, Stern, F., 2020. FSI and MDO for Weight Reduction of a Grillage Panel of a Fast Deep-V Planing Hull Subject to Slamming in Waves. *In*: 33rd Symposium on Naval Hydrodynamics

El-Reedy, M.A., 2021. *Offshore Projects and Engineering Management*. 1st Edition. USA: Gulf Professional Publishing

Ghadimi, P., Tavakoli, S., Dashtimanesh, A., 2017. Calm Water Performance of Hard-Chine Vessels in Semi-Planing and Planing Regimes. *Polish Maritime Research*, Volume 23(4), pp. 23–45

Islam, H., Soares, C.G., 2019. Effect of Trim on Container Ship Resistance at Different Ship Speeds and Drafts. *Ocean Engineering*, Volume 183, pp. 106–115

International Maritime Organization (IMO), 2016. Module 4 – Ship Board Energy Management. In *IMO Train the Trainer (TTT) Course on Energy Efficient Ship Operation*, pp. 17–19. Available online at https://wwwcdn.imo.org/localresources/en/OurWork/Environment/Documents/Air pollution/M4 energy management onboard final.pdf.

International Towing Tank Conference (ITTC), 2017. ITTC-Recommended Procedures and Guidelines: Uncertainty Analysis in CFD Verification and Validation Methodology and Procedures. *In*: 28th International Towing Tank Conference, pp. 17–22

International Towing Tank Conference (ITTC), 2014a. ITTC-Recommended Procedures and Guidelines: Practical Guidelines for Ship Resistance CFD No. 7.5–03–02–04. *In*: 27th International Conference Towing Tank, pp. 1–12

International Towing Tank Conference (ITTC), 2014b. ITTC-Recommended Procedures and Guidelines: Example for Uncertainty Analysis of Resistance Tests in Towing Tanks (7.5-02-02-02.1), *In*: 27th International Conference Towing Tank. pp. 1–11

International Towing Tank Conference (ITTC), 2014c. ITTC-Recommended Procedures and

Guidelines: General Guideline for Uncertainty Analysis in Resistance Tests 7.5-02-02-02 (Revision 02). *In*: 27th International Conference Towing Tank

Karanassos, H.A., 2016. *Commercial Ship Surveying: On/Off Hire Condition Surveys and Bunker Surveys*. UK: Elsevier

Kazemi, H., Salari, M., 2017. Effects of Loading Conditions on Hydrodynamics of a Hard-Chine Planing Vessel Using CFD and a Dynamic Model. International Jounal of Maritime Technology, Volume 7, pp. 11–18

Latorre, R., 2003. Naval Architecture. In: *Encyclopedia of Physical Science and Technology*, Third Edition, Academic Press, USA, pp. 343–360

Le, T.-H., Vu, M.T., Bich, V.N., Phuong, N.K., Ha, N.T.H., Chuan, T.Q., Tu, T.N., 2021. Numerical Investigation on the Effect of Trim on Ship Resistance by RANSE Method. *Applied Ocean Research*, Volume 111, p. 102642

Luhulima, R. B., Sutiyo, Alia, M. R., Utama, I.K.A.P., 2021. Experimental Investigation into the Resistance Characteristics of Trimaran and Pentamaran Configurations. *International Journal of Technology*, Volume 12(5), pp. 291–319

Lyu, X., Tu, H., Xie, D., Sun, J., 2018. On Resistance Reduction of a Hull by Trim Optimization. Brodogr. *Brodogradnja*, Volume 69(1), pp. 1–13

Marintek, 2021. Marine Customer Cases. NUMECA International. Available online at https://www.numeca.com/marine-case/id/129, Accessed on September 29, 2021

Menter, F.R., 1994. Two-Equation Eddy-Viscosity Turbulence Models for Engineering Applications. *AIAA Journal*, Volume 32(8), pp. 1598–1605

Molland, A.F., Turnock, S.R., Hudson, D.A., 2017. Components of Hull Resistance. In: *Ship Resistance and Propulsion*, 2nd Edition, Cambridge University Press, Cambridge, pp. 12–69

Molland, A.F., Turnock, S.R., Hudson, D.A., Utama, I.K.A.P., 2014. Reducing Ship Emissions: A Review of Potential Practical Improvements in the Propulsive Efficiency of Future Ships. *Transactions of The Royal Institution of Naval Architects Part A: International Journal of Maritime Engineering,* Volume 156 (A2), p. 175

Reichel, M., Minchev, A., Larsen, N.L., 2014. Trim Optimisation-Theory and Practice. *TransNav: International Journal on Marine Navigation and Safety of Sea Transportation*, Volume *8,* pp. 387–392

Savitsky, D., 2003. On the Subject of High-Speed Monohulls. *In*: Presented to the Greek Section Of the Society Of Naval Architects and Marine Engineers, Grecee, pp. 1–44

Sherbaz, S., Duan, W., 2014. Ship Trim Optimization: Assessment of Influence of Trim on Resistance of MOERI Container Ship. *The Scientific World Journal,* Volume 2014. https://doi.org/10.1155/2014/603695

Suastika, K., Hidayat, A., Riyadi, S., 2017. Effects of the Application of a Stern Foil on Ship Resistance: a Case Study of an Orela Crew Boat. *International Journal of Technology,* Volume 8(7), pp. 1266–1275

Utama, I.K.A.P., Sutiyo, Suastika, I.K., 2021a. Experimental and Numerical Investigation into the Effect of the Axe-Bow on the Drag Reduction of a Trimaran Configuration. *International Journal of Technology,* Volume 12 (3), pp. 527–538

Utama, I.K.A.P., Purnamasari, D., Suastika, I.K., Nurhadi, Thomas, G.A., 2021b. Toward Improvement of Resistance Testing Reliability. *Journal of Engineering and Technological Sciences*, Volume 53(2), pp. 201–210